Numerical investigation on quantum-confined stark effect and polarization effect of short-wavelength LEDs

WANG DANGHUI[1,*], HAN YE[1], XU TIANHAN[1], ZHANG YANG[2]
[1]*College of New Energy of Xi'an Shiyou University, Xi'an 710065, China*
[2]*Longgi Green Energy Technology Co., Ltd, Block B, No.8989 Shangji Road, Economic and Technological Development Zone, Xi'an, China*

Due to the intrinsic properties of larger-mismatched, stronger-polarization and non-equilibrium growth, the efficiency-droop effect has been a critical obstacle to improve the quantum efficiency of III-nitride short-wavelength LEDs under high current density. Quantum-Combined Stark Effect induced by built-in electric field existed within the active region of LEDs plays a key role to reduce the quantum efficiency and causes a redshift of luminous wavelength subsequently. In this study, the light output power, bandgap diagrams, radiative recombination efficiencies, carries concentrations, spontaneous emission properties and electrical properties of InGaN/AlGaN violet LEDs with different polarities (c-plane, m-plane and r-plane) at high current density of 600 A/m are investigated using APSYS software. Conclusions indicate that all the parameters of luminescence properties and electrical properties have strong dependence on the high current density of 600 A/m, which is contributive to eliminate the quantum-confined Stark effect and enhance the luminescence efficiency of polarity short-wavelength LEDs. The results of this paper provide theoretical bases for further optimizing and designing the active region and enhancing the luminous efficiency of short-wavelength LEDs.

(Received March 21, 2022; accepted February 6, 2023)

Keywords: LED, Polarization effect, Efficiency-droop effect, Non-polarity

1. Introduction

Wide-bandgap gallium nitride (GaN) based semiconductor material system has excellent luminous properties and electrical properties owing to its direct bandgap, higher radiative-recombination efficiency and carrier mobility, which covering wavelength range from IR to UV and becoming the key promising materials in the fabrication of light-emitting diodes (LED), laser diodes (LD), and blue-violet to infrared radiation detectors [1-4]. In recent years, great innovation in solid-state lighting technology, especially for short-wavelength blue/UV LED. Owing to its high brightness and power, blue/UV LEDs are now widely used in lithography technology, water purification, disinfection, sterilization, security screening and bacteria inactivated [5-9]. According to the relevant research, the COVID-19 virus is sensitive to UV LEDs. After exposure in UV LEDs with wavelength in the range of 240-280 nm is an effective method to kill the virus. The novel coronavirus reported a 99.99% UV lethal dose of 1445 mJ/cm^2, which is much higher than that of the SARS-CoV UV of 324 mJ/cm^2 [10]. To prevent the spread of the novel coronavirus, GaN-based blue/UV LEDs with higher-power, high reliability, and long-lifetime are urgently developed. To obtain higher luminous efficiency, short-wavelength LEDs must operate at higher current densities. However, the efficiency-droop effect under the synergistic action of high current injection, large mismatch, and strong polarization has become the key factor impeding the applications of short-wavelength LEDs [11-14]. Studies still have not formed a unified understanding of the origins and mechanisms of the efficiency-droop effect of short-wavelength LEDs. Due to the inherent characteristics of larger-mismatched, stronger-polarization, and non-equilibrium growth, the crystalline quality of heteroepitaxial thin films and the built-in electric field induced by polarity materials are the key factors affecting the properties, quality, and reliability of LEDs. On the one hand, due to the differences between lattice parameters and thermal expansion coefficient of substrate, there exists a higher dislocation density (including point defects, threading dislocations, etc.) in the epitaxial thin films, which reduces the probability of radiation recombination and carrier mobility. On the other hand, the stronger polarization effect (including the spontaneous polarization and piezoelectric polarization) in the active region and subsequently the quantum-confined Stark effect induced by the built-in electric field make a redshift of wavelength, which degrades the external quantum efficiency of LEDs.

Many of research have reported to improve the efficiency-droop effect of short-wavelength LEDs under high current density injection. The consensus among researchers are that high electronic leakage, poor hole

injection, delocalization of carriers and the non-radiative recombination of Auger electrons that cause the efficiency droop under high current injection [15-18]. The polarization effect is one of the main reasons of electron leakage and the low efficiency of hole injection. The best candidate way to eliminate or avoid the influence of the polarization effect is using semi-polar or non-polar active region in LEDs [19-21], such as growing on m-plane (semi-polar) or r-plane (non-polar) sapphire substrates. P. Altereit et al. successfully grew m-plane GaN on γ-$LiAlO_2$ (100) plane by molecular beam epitaxy (MBE) [22]. Nakamura et al. studied the distribution of defects in a-plane heteroepitaxy GaN using SIMS, TEM, and PAS and proposed an orientation-dependent defect model based on dynamics to explain the correlation of defect concentration between a-plane MOCVD GaN and a-plane HVPE GaN [23]. Sung-Min Hwang et al. successfully grew high crystalline quality non-polar a-plane GaN thin films with fine specular surfaces on r-plane sapphire substrates. The FWHM of XRC was 407 arcsec along the c-axis, and the root mean square (RMS) was 1.23 nm. The PL peak located at wavelength of 477 nm [24] of a non-polar a-plane GaN LED grown on the a-GaN template. Xu Shengrui et al. have grown non-polar Si-doped a-plane GaN films on r-plane sapphire (Al_2O_3) substrates and studied the optical properties and electrical properties using PL, high-resolution X-ray diffractometer (HRXRD), atomic force microscopy (AFM) and Hall measurement. In this paper, APSYS software was employed to simulate the InGaN/AlGaN multi-quantum well blue/ violet LED with different polarities (c-plane, m-plane and r-plane). We analyze the luminescence properties, carrier concertation, bandgap diagram, radiative recombination efficiency, ideality factors and investigated the polar c-plane LEDs in details, specially explored the influence factors of polarization effect on efficiency-droop effect of polarity, semi-polarity and non-polarity LEDs.

2. Models and simulation of LEDs

In order to improve the luminescence properties of LED under high current density injection, the main issues are to weaken/eliminate the effect of polarization built-in electric field, release/regulate the residual stress exists in the active region and reduce the threading dislocation density. In this study, APSYS simulation software is used to design the InGaN/AlGaN multi-quantum well blue/violet LEDs with different polarity (c-plane, m-plane and r-plane). Fig. 1 shows the schematic diagram of LED structure simulated. The devices were grown on (0001) orientation. The structure consisted of an n-type AlGaN layer with the thickness of 4 μm (doping concentration is 5×10^{18} cm^{-3}) and 7-period with thickness of 3 nm $In_{0.1}Ga_{0.9}N$/10 nm $Al_{0.1}Ga_{0.9}N$ multi-quantum well. The following electron blocking layer (EBL) is a 20 nm thick p-$Al_{0.2}Ga_{0.8}N$ layer followed by an p-type GaN layer with the thickness of 0.2 μm (doping concentration: 5×10^{20} cm^{-3}). The growth direction of sample A, B and C are represented c-plane, m-plane and r-plane respectively, and the area of the simulator parts are 350 μm × 350 μm.

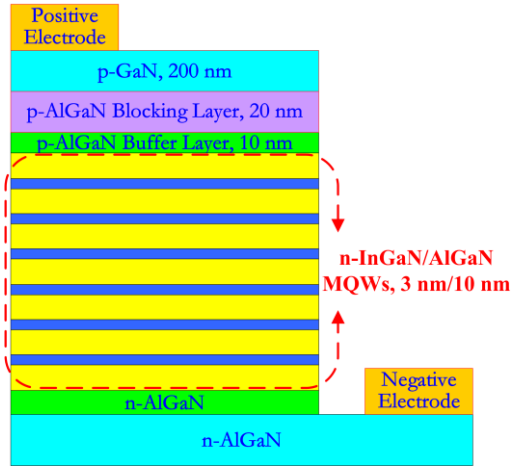

Fig. 1. LED structure diagram (color online)

3. Results and discussions

3.1. Luminescence properties

Fig. 2 shows the simulation results of the light output power of the three LED samples with the increasing of injection current density. As can be seen from Fig. 2, the light output power of the three samples show a similar tendency with the increasing injection current density, and the curves of sample B and C increase faster than sample A. At low current density, there is little differences among the three samples in light output power, and with the increasing current density, the larger difference in light output power among the three samples. The non-polarity sample C has the best light output power characteristics, and its light output power is 2.56 times that of sample A at current density of 600 A/m. The light output power of the three LEDs at the current density of 600 A/m are shown in Table 1.

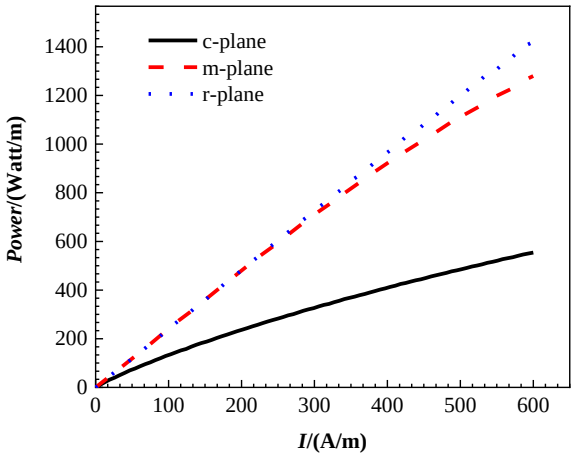

Fig. 2. Relationships of light output power of the three samples with current density (color online)

Table 1. Light output power at current density of 600 A/m

Sample	A	B	C
Output power (*W*/m)	554	1280	1420
Multiple of Sample A	1	2.31	2.56

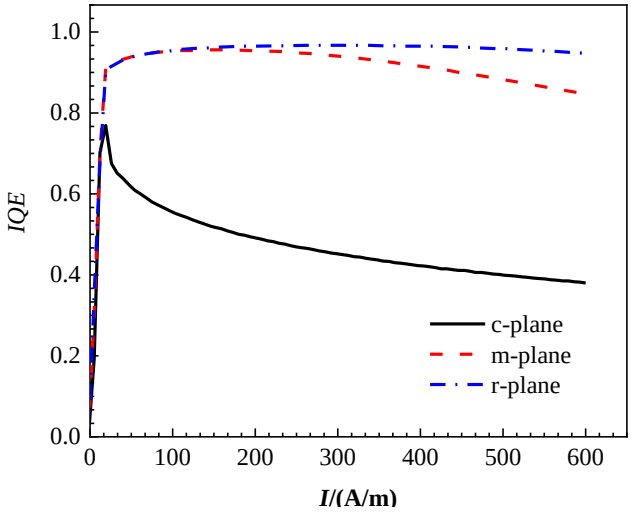

Fig. 3. The current density dependence of the internal quantum efficiency of the three samples (color online)

Fig. 3 shows the current density dependence of the internal quantum efficiency (IQE) of the three samples. As can be seen from Fig. 3, the IQE of all the samples reach rapidly its maximum value when the current is small, and the maximum values of IQE of sample B and sample C are much higher than those of sample A. With the increasing of the injection current density, there is a more obvious efficiency steep drop in sample A, while the efficiency drop in sample B is smaller, and sample C has basically no efficiency-droop effect. The efficiency droop factor is used to define as $(IQE_{max}\text{-}IQE_{600A/m})/IQE_{max}$ to character the efficiency-droop effect. The efficiency droop factors of the three samples are calculated as shown in Table 2 Comparing the efficiency droop factor of the three samples, it can be seen that the non-polarity and semi-polarity multiple quantum wells significantly are beneficial to efficiency-droop effect of GaN-based blue/violet LEDs.

Table 2. The efficiency-droop factors of the three samples

Sample	A	B	C
Efficiency-Droop Factor（%）	50.60	11.30	1.96

In order to investigate the mechanisms of quantum-confined Stark efficiency with the increasing current density, Fig. 4 shows the bandgap diagrams of the three samples at injection current density of 600 A/m.

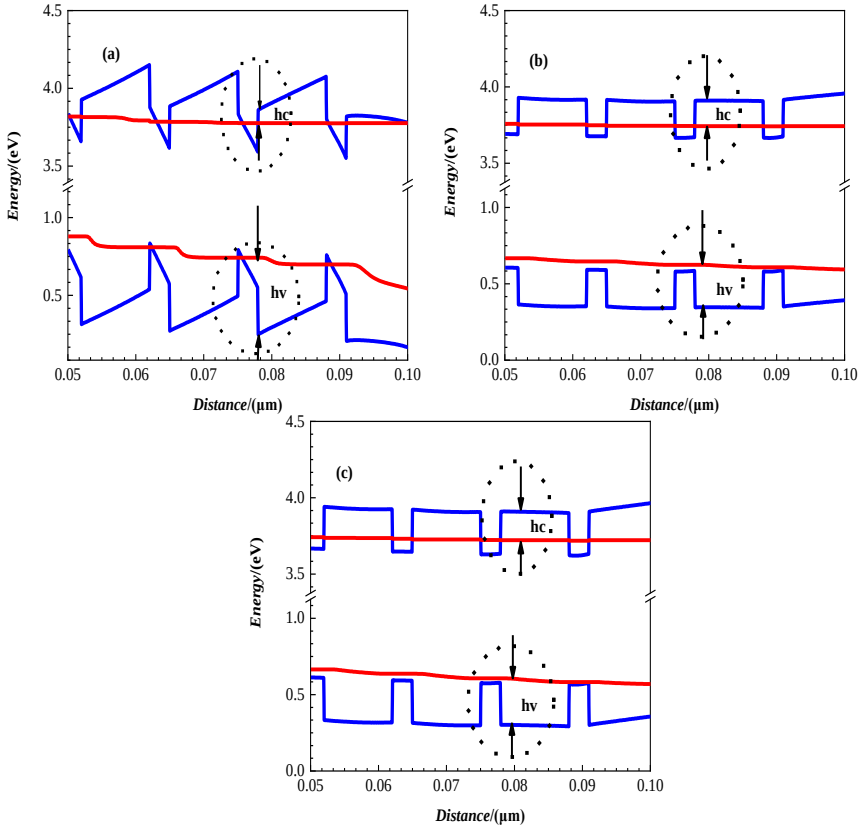

Fig. 4. Effective barrier height of electron (hc) and hole effective (hv) of the three samples under the injection current density of 600 A/m: (a) sample A; (b) sample B and (c) sample C (color online)

From Fig. 4(a), (4b) and (4c), one can see that sample A has an internal electric field due to the polarization effect, which induces the bandgap to bend, and the existence of the built-in electric field leads to the electron leakage and reduces the probability of radiation recombination. As well known, carriers in sample A are gather on both sides of the quantum well, and the recombination of electrons and holes occurs in the last quantum well. Fig. 5(a) shows the carriers concentration of the three samples at current density of 600 A/m. From Fig. 5(b), we can see that the electron and hole concentrations in several quantum wells near the n-type region are very low, which is one of the main reasons for the efficiency-droop effect. Compared with sample A, the bandgap tilting phenomena in sample B and sample C have been weakened. Driven by electric field, electrons and holes move toward the center of the quantum well, which increases the overlap of electron and hole wave functions. The overlap integral values of electron wavefunctions and hole wavefunctions of the three studied devices were 36.9%, 65.8% and 83.7% respectively, which indicates that the active region with semi-polarity and non-polarity can effectively improve the overlap rate of electron-hole wavefunctions. In addition, compared with sample A, the concentration of electrons and holes in the quantum wells near the n-type region increase faster in sample B and sample C than that in sample A, which demonstrates that the nonpolar and semi-polar samples improve the hole injection efficiency by limiting the escape of electrons and lead to a significantly higher carrier concentration in sample B and sample C than that in sample A.

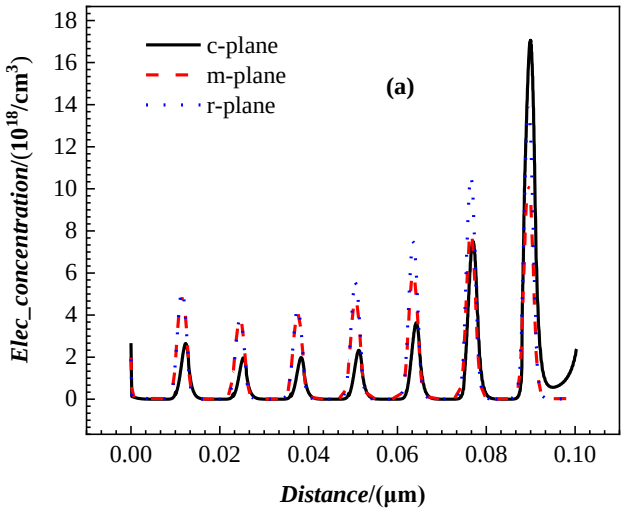

Fig. 5(a). Electron concentration in the active region under injection current of 600 A/m (color online)

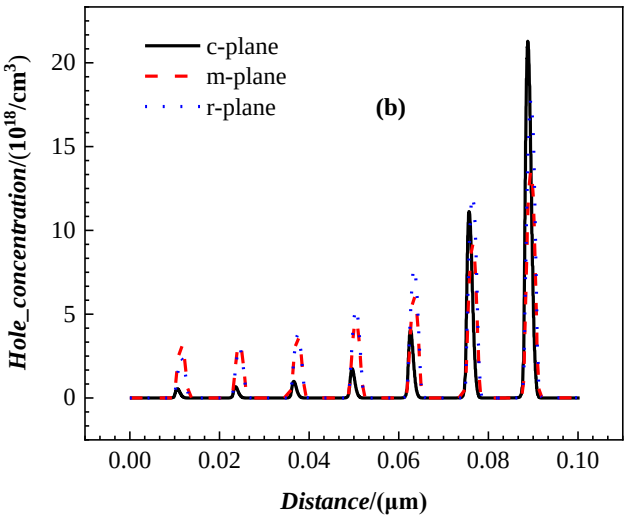

Fig. 5(b). Hole concentration in the active region under current density of 600 A/m (color online)

To quantitatively the physical mechanisms of quantum-confined Stark effect, the effective heights of potential wells and potential barriers in the active region of the three samples were calculated (the conduction band potential barrier height was set to hc and the valence band potential barrier height was set to hv) as shown in Fig. 4 and Table 3. As can be seen from Table 3, the hc of the conduction bands and the potential height of the electron blocking layer of sample B and sample C are higher compared to sample A, which indicates that the nonpolar and semi-polar multiple quantum wells weaken the effect of the built-in electric field and restrain the electron leakage. In additional, higher height of the electron blocking layer in Sample B and Sample C can effectively reduce the leakage current of LEDs. On the other hand, the hv of valence bands of sample B and sample C are lower than that of sample A, which also indicates that the lower barrier height enhances the injection efficiency of hole. Therefore, using the nonpolar or semi-polar multiple quantum well effectively weakens/eliminates the bandgap bending induced by the polarization effect, and reduces the electron leakage and low hole injection efficiency at higher current density.

Table 3. Quantum well potential well heights of three samples

Sample	Conduction band barrier height *hc*/meV	Valence band barrier height *hv*/meV	Electron blocking layer height *hc*/meV
A	90	483	53
B	169	288	179
C	192	305	193

The radiation recombination rates of the three samples at the current density of 600 A/m are shown in Fig. 6. As can be seen from Fig. 6, the radiative recombination rates of sample B and sample C are larger than sample A. In additional, in n-type region the radiative recombination rate of sample A is almost zero, which is due to electron leakage, lower hole injection and lower wave function overlap and higher quantum efficiency in sample B and sample C. This also confirms the above carrier concentration and indicates that the samples using nonpolar quantum wells to enhance the luminescence properties of the samples by improving the carrier concentration in the active region and increasing the wave function overlap ratio of electrons and holes, and improving the radiation recombination efficiency.

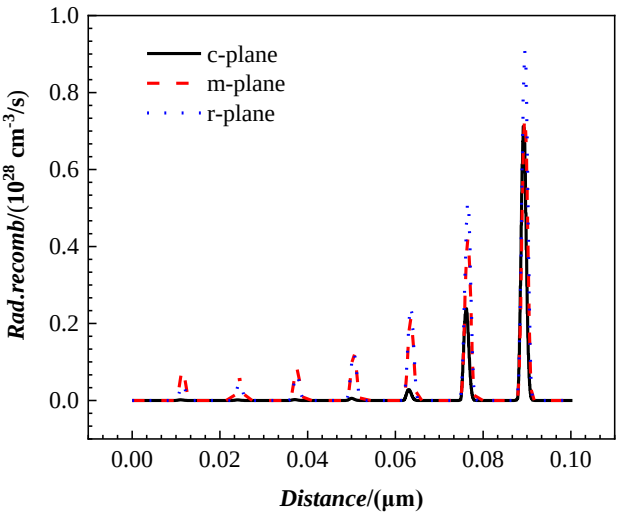

Fig. 6. Radiation recombination rates of three samples at the current density of 600 A/m

The spontaneous emission spectrum of the three samples at the current density of 600 A/m shown in Fig. 7. From Fig. 7, one can see that emission wavelengths of sample A and sample B have obvious redshifts, which is due to exist the built-in electrical field induced by the polarization effect in sample A, while sample C is almost not affected by the polarization effect. From Table 4 the spontaneous emission spectrum intensity of sample B and sample C are significantly higher than that of sample A. The peak of spontaneous emission spectrum of sample B is 2.15 times than sample A, and sample C is 2.68 times than sample A.

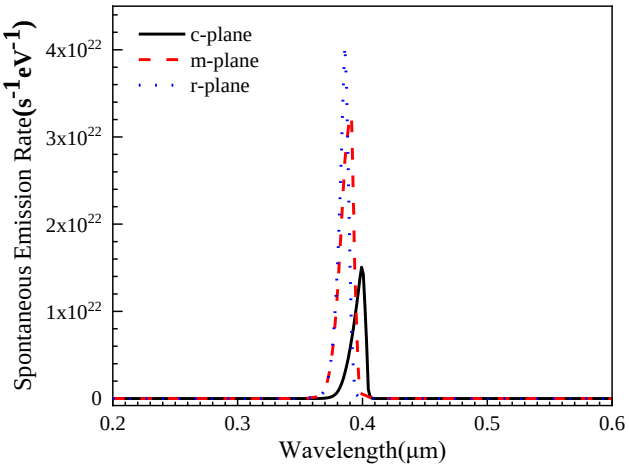

Fig. 7. Spontaneous emission spectra of three samples at current density of 600 A/m (color online)

Table 4. Spontaneous emission spectra of three studied samples

Sample	A	B	C
Spontaneous emission rate ($\times 10^{22} s^{-1} eV^{-1}$)	1.51	3.25	4.05

3.2. Analysis of electrical characteristics of LED

The I-V curves and ideality factor n are related to the radiative/nonradiative recombination mechanisms and lifetime and reliability of LEDs. The I-V equation of LEDs is shown in Equation (1):

$$I = I_s(e^{\frac{qV}{nk_BT}} - 1) \quad (1)$$

Here, I_s is the reverse saturation current, k_B is the Boltzmann constant, and T is the Kelvin temperature. According to the Sah-Noyce-Shockley model, in p-n junction, the diffusion current plays a dominant role for the ideality factor n=1 and the recombination current plays a dominate role for the ideality factor n=2 [25]. For GaN-based LEDs, the ideality factor n>2, which cannot be explained using the diffusion-recombination theory but the trap-assisted tunneling theory [26-30]. The I-V curve of sample A is shown in Fig. 8 (sample B and sample C have the similar tendency as sample A), and the ideality factor n can be extracted by fitting the I-V curve with equation (1), and the calculated results are shown in Table 5. From Table 5, we can see that the ideality factors of the three samples are much larger than 2 which means that the tunneling current becomes more important at high current density [25].

Table 5. Ideality factors of the three studied LEDs

Sample	A	B	C
Ideality Factor n	6.38	7.23	7.31

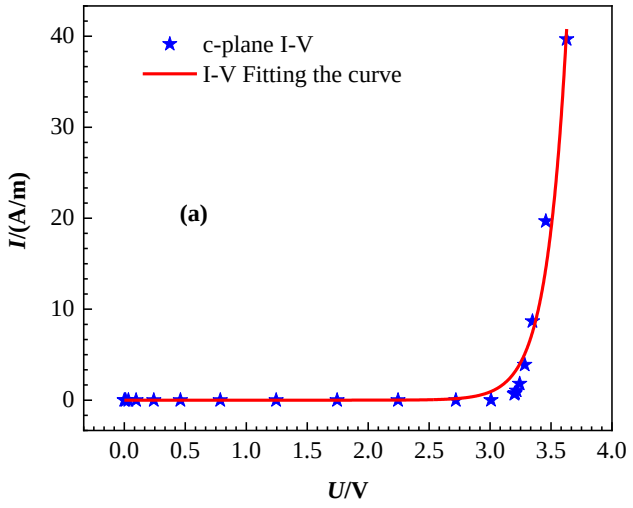

Fig. 8. I-V curve of sample A (color online)

4. Conclusions

In this study, the light output power, bandgap diagrams, radiative recombination properties, carries concentrations, spontaneous emission properties and electrical properties of GaN-based blue/violet LEDs with non-polarity (r-plane), semi-polarity (m-plane) and polarity (c-plane) were investigated using APSYS software. The results show that the parameters of the luminescence properties and electrical properties have strong dependence on the high current density of 600 A/m in the polarity/semi-polarity active region of the short wavelength LEDs, which is caused by the polarization effect and quantum-confined Stark effect.

References

[1] H. C. Tao, S. R. Xu, J. Ch. Zhang, P. X. Li, Z. Y. Lin, Y. Hao, IEEE Transactions on Electron Devices **66**(1), 478 (2019).
[2] Huake Su, Shengrui Xu, Hongchang Tao, Xiaomeng Fan, Jinjuan Du, Ruoshi Peng, Ying Zhao, Lixia Ai, Haoyang Wu, Jincheng Zhang, Peixian Li, Hao Yue, IEEE Electron Device Letters **42**(9), 1346 (2021).
[3] Muhammad Usman, Urooj Mushtaq, Dong-Guang Zheng, Dong-Pyo Han, Nazeer Muhammad, Materials Research Express **6**(4), 045909 (2019).
[4] Kevin J. Chen, Oliver Häberlen, Alex Lidow, Chun Lin Tsai, Tetsuzo Ueda, Yasuhiro Uemoto, Yifeng Wu, IEEE Transactions on Electron Devices **64**(3), 779 (2017).
[5] Takayoshi Takano, Takuya Mino, Jun Sakai, Norimichi Noguchi, Kenji Tsubaki, Hideki Hirayama, Applied Physics Express **10**(3), 031002 (2017).
[6] Joachim Piprek, Optical and Quantum Electronics **44**(3), 67 (2012).
[7] J. Han, M. H. Crawford, R. J. Shul, J. J. Figiel, M. Banas, L. Zhang, Applied Physics Letters **73**(12), 1688 (1998).
[8] Hideki Hirayama, Norimichi Noguchi, Tohru Yatabe, Norihiko Kamata, Applied Physics Express **1**(5), 051101 (2008).
[9] Yoshitaka Taniyasu, Makoto Kasu, Toshiki Makimoto, Nature **441**(7091), 325 (2006).
[10] Jian Chen, Stephanie Loeb, Jae-Hong Kim, Environmental Science: Water Research & Technology **3**(2), 188 (2017).
[11] Houqiang Fu, Zhijian Lu, Yuji Zhao, AIP Advances **6**(6), 065013 (2016).
[12] Min-Ho Kim, Martin F. Schubert, Qi Dai, Jong Kyu Kim, E. Fred Schubert, Joachim Piprek, Yongjo Park, Applied Physics Letters **91**(18), 183507 (2007).
[13] Martin F. Schubert, Jiuru Xu, Jong Kyu Kim, E. Fred Schubert, Min Ho Kim, Sukho Yoon, Soo Min Lee, Cheolsoo Sone, Tan Sakong, Yongjo Park, Applied Physics Letters **93**(4), 041102 (2008).
[14] Cao Dong-Xing, Guo Zhi-You, Liang Fu-Bo, Yang Xiao-Dong, Huang Hong-Yong, Acta Phys. Sin. **l61**(13), 511 (2012).
[15] Lai Wang, Xiao Meng, Jiaxing Wang, Zhibiao Hao, Yi Luo, Changzheng Sun, Yanjun Han, Bing Xiong, Jian Wang, Hongtao Li, arXiv preprint arXiv:1611.07972 (2016).
[16] Muhammad Usman, Shahzeb Malik, M. Ajmal Khan, Hideki Hirayama, Nanotechnology **32**, 215703 (2021).
[17] N. Poyiatzis, M. Athanasiou, J. Bai, Y. Gong, T. Wang, Scientific Reports **9**(1), 1 (2019).
[18] Zhe Zhuang, Daisuke Iida, Kazuhiro Ohkawa, Optics Express **28**(21), 30423 (2020).
[19] Jianfeng Yan, Zhang Jie, Guo Liwei, Zhu Xueliang, Peng Mingzeng, Jia Haiqiang, Chen Hong, Zhou Junming, Chinese J. Semiconductors **28**(10), 1562 (2007).
[20] Hongfeng Jia, Huabin Yu, Yang Kang, Zhongjie Ren, J. Applied Physics **129**(13), 133102 (2021).
[21] Shudan Xiao, Huabin Yu, Hongfeng Jia, Muhammad Hunain Memon, Rui Wang, Haochen Zhang, Haiding Sun, Optics Letters **47**(16), 4187 (2022).
[22] P. Waltereit, O. Brandt, A. Trampert, H. T. Grahn, J. Menniger, M. Ramsteiner, M. Reiche, K. H. Ploog, Nature **406**(6798), 865 (2000).
[23] Filip Tuomisto, T. Paskova, T. Kröger, S. Figge, D. Hommel, B. Monemar, R. Kersting, Applied Physics Letters **90**(12), 121915 (2007).
[24] Sung-Min Hwang, Yong Gon Seo, Kwang Hyeon Baik, In-Sung Cho, Jong Hyeob Baek, Sukkoo Jung, Tae Geun Kim, Meoungwhan Cho, Applied Physics Letters **95**(7), 071101 (2009).
[25] Danghui Wang, Tianhan Xu, Acta Phys. Sin. **68**(12), 104 (2019).

[26] Chih-Tang Sah, Robert N. Noyce, William Shockley, Proceedings of the IRE **45**(9), 1228 (1957).
[27] H. C. Casey Jr, John Muth, Sheeba Krishnankutty, J. M. Zavada, Applied Physics Letters **68**(20), 2867 (1996).
[28] Piotr Perlin, M. Osiński, P. Eliseev, V. Smagley, J. Mu, M. Banas, P. Sartori, Applied Physics Letters **69**(12), 1680 (1996).
[29] X. A. Cao, E. B. Stokes, P. M. Sandvik, S. F. LeBoeuf, J. Kretchmer, D. Walker, IEEE Electron Device Letters **23**(9), 535 (2002).
[30] K. Mayes, A. Yasan, R. McClintock, D. Shiell, S. R. Darvish, P. Kung, M. Razeghi, Applied Physics Letters **84**(7), 1046 (2004).

*Corresponding author: wdhyxp@outlook.com